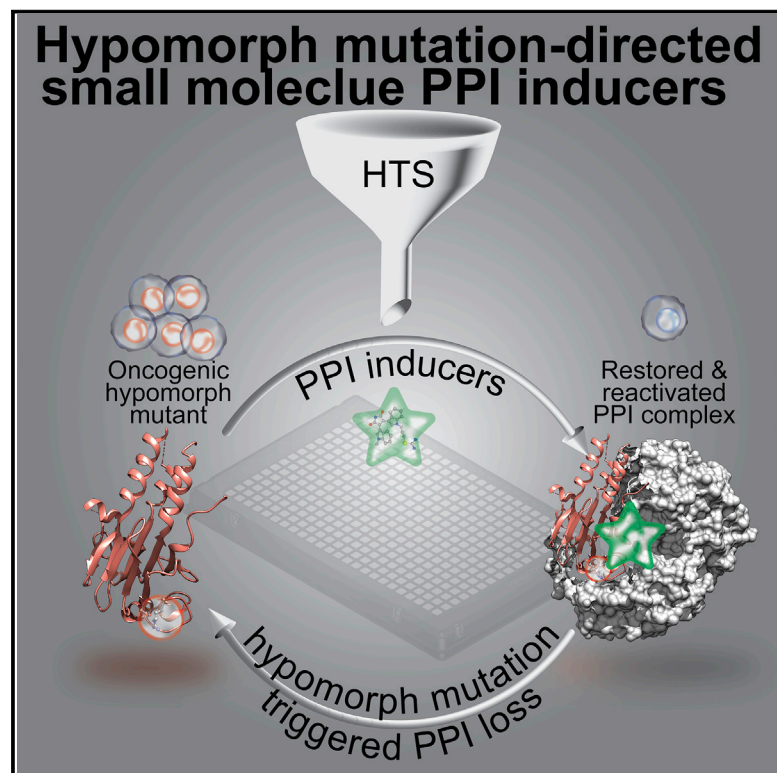# Cell Chemical Biology

Hypomorph mutation-directed small-molecule protein-protein interaction inducers to restore mutant SMAD4-suppressed TGF-β signaling

Graphical Abstract

Authors
Cong Tang, Xiulei Mo, Qiankun Niu, ..., Andrey A. Ivanov, Yuhong Du, Haian Fu

Correspondence
xmo@emory.edu (X.M.), hfu@emory.edu (H.F.)

In Brief

Tang et al. report a systematic approach for unbiased discovery of small-molecule protein-protein interaction (PPI)-inducing activators as molecular glues to enhance PPIs that are attenuated by hypomorph mutations and as chemical probes for biological insights and therapeutic discovery.

Highlights

- A TR-FRET assay recapitulates variant-directed SMAD4/SMAD3 PPI dynamics

- uHTS reveals small-molecule SMAD4^{MUT}/SMAD3 PPI inducers as targeted molecular glues

- Bisindolylmaleimides derivatives restore SMAD4^{MUT}/SMAD3 interaction

- SMAD4^{MUT}/SMAD3 PPI inducers reestablish tumor-suppressive TGF-β signaling

CellPress

Article

Hypomorph mutation-directed small-molecule protein-protein interaction inducers to restore mutant SMAD4-suppressed TGF-β signaling

Cong Tang,[1,2,5] Xiulei Mo,[1,5,*] Qiankun Niu,[1] Alafate Wahafu,[1,2] Xuan Yang,[1,3] Min Qui,[1,3] Andrey A. Ivanov,[1,3] Yuhong Du,[1,3] and Haian Fu[1,3,4,6,*]

[1]Department of Pharmacology and Chemical Biology, Emory University School of Medicine, Atlanta, GA 30322, USA
[2]The First Affiliated Hospital, Medical School of Xi'an Jiaotong University, Xi'an, Shannxi 710061, P.R.China
[3]Emory Chemical Biology Discovery Center, Emory University School of Medicine, Atlanta, GA 30322, USA
[4]Department of Hematology and Medical Oncology and Winship Cancer Institute, Emory University, Atlanta, GA 30322, USA
[5]These authors contributed equally
[6]Lead Contact
*Correspondence: xmo@emory.edu (X.M.), hfu@emory.edu (H.F.)
https://doi.org/10.1016/j.chembiol.2020.11.010

SUMMARY

Tumor suppressor genes represent a major class of oncogenic drivers. However, direct targeting of loss-of-function tumor suppressors remains challenging. To address this gap, we explored a variant-directed chemical biology approach to reverse the lost function of tumor suppressors using SMAD4 as an example. SMAD4, a central mediator of the TGF-β pathway, is recurrently mutated in many tumors. Here, we report the development of a TR-FRET technology that recapitulated the dynamic differential interaction of SMAD4 and SMAD4^{R361H} with SMAD3 and identified Ro-31-8220, a bisindolylmaleimide derivative, as a SMAD4^{R361H}/SMAD3 interaction inducer. Ro-31-8220 reactivated the dormant SMAD4^{R361H}-mediated transcriptional activity and restored TGF-β-induced tumor suppression activity in SMAD4 mutant cancer cells. Thus, demonstration of Ro-31-8220 as a SMAD4^{R361H}/SMAD3 interaction inducer illustrates a general strategy to reverse the lost function of tumor suppressors with hypomorph mutations and supports a systematic approach to develop small-molecule protein-protein interaction (PPI) molecular glues for biological insights and therapeutic discovery.

INTRODUCTION

Cancer genomics studies have revealed a vast landscape of genetic alterations in human malignancies (Vogelstein et al., 2013). Gain-of-function alterations in oncogenes, such as kinases, offer defined targets that drive small-molecule inhibitor-based therapeutic discovery (Zhang et al., 2009). However, the loss-of-function alterations in tumor suppressor genes remain to be considered as "undruggable" due to the challenges in restoring their impaired tumor-suppressive functions. Therefore, the undrugged tumor suppressor space presents a daunting task, as well as unprecedented opportunities, for small-molecule therapeutic discovery (Guo et al., 2014; Zhao and DePinho, 2017).

The tumor suppressor gene *SMAD4* is a core mediator of the canonical transforming growth factor β (TGF-β) signaling pathway (Massague, 2012; Miyaki and Kuroki, 2003; Zhao et al., 2018). Upon TGF-β stimulation, SMAD4 forms a heteromeric transcriptional complex with other SMADs, such as SMAD3, and acts as a pivotal switch to transduce the extracellular signals to the nucleus (Chacko et al., 2004; Nakao et al., 1997). Although the TGF-β pathway has a paradoxical role in

suppressing and promoting tumor growth depending on its context, inactivating SMAD4 mutations have been recurrently identified in a range of solid tumors, such as pancreatic and colon cancers (Blackford et al., 2009; MacGrogan et al., 1997; Massague, 2012; Salovaara et al., 2002; Woodford-Richens et al., 2001). SMAD4 R361H mutation, one of the hotspot missense mutations in the MH2 domain, impairs the protein-protein interaction (PPI) between SMAD4 and SMAD3, leading to the disruption of the transcriptional complex, and blocking TGF-β-induced anti-proliferation signaling (Fleming et al., 2013). Despite the promising therapeutic potential offered by these SMAD4 inactivation mutations, targeting such hypomorphic interactions to restore their wild-type (WT) function remains highly challenging, particularly using small-molecule approaches.

To address this critical gap in small-molecule PPI modulator discovery to re-gain the desired function of the undruggable tumor suppressor SMAD4, we developed a general high-throughput screening approach to identify small molecules that can induce and stabilize the interaction of SMAD3 with mutated SMAD4 to provide a proof of concept. Here, we report the development of a time-resolved fluorescence resonance energy
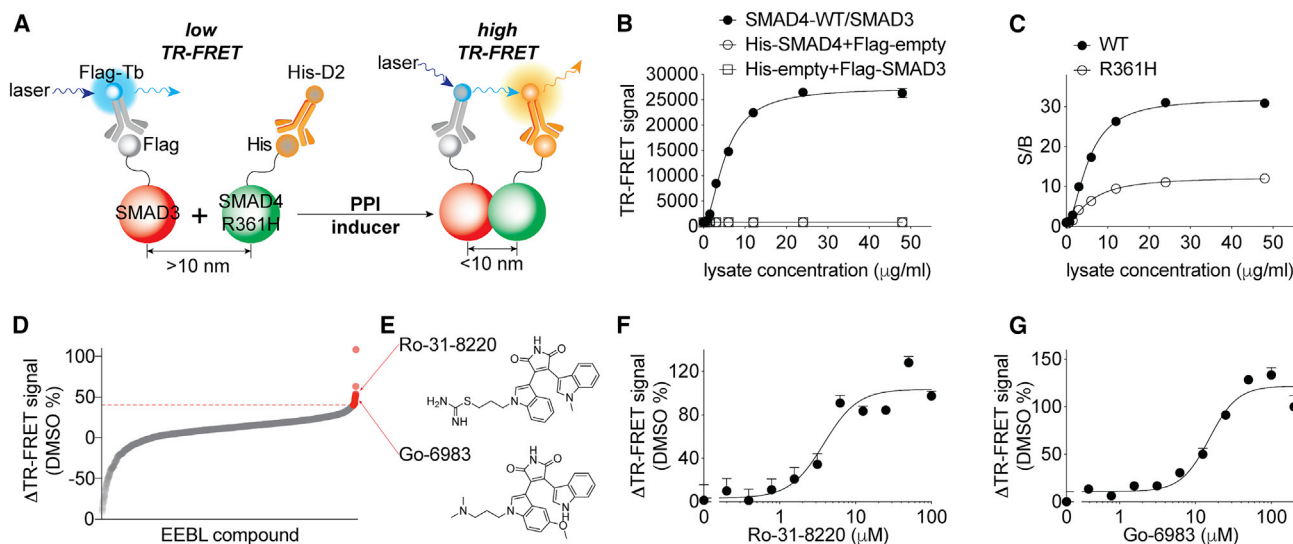
Figure 1. Identification of Ro-31-8220 as a small-molecule inducer for SMAD4^{R361H}/SMAD3 PPI

(A) Schematic illustration of the design of the TR-FRET assay for monitoring the SMAD4/SMAD3 PPI to discover small-molecule PPI inducers. Anti-Flag-Tb coupled with Flag-SMAD3 serves as the TR-FRET donor and anti-His-D2 coupled with His-SMAD4^{R361H} serves as the acceptor. At the basal level, R361H impairs SMAD4 interaction with SMAD3, yielding low TR-FRET signal. Upon treatment with a PPI inducer, the induced SMAD3/SMAD4^{R361H} complex formation brings two fluorophores into close proximity (<10 nm), generating a high TR-FRET signal.

(B) Dose-dependent TR-FRET signals of the SMAD4^{WT}/SMAD3 PPI. The cell lysate from the HEK293T cells expressing the His-SMAD4^{WT} and Flag-SMAD3 or the empty vector controls were serial diluted as indicated. The data are presented as mean ± SD from a representative experiment.

(C) Dynamic assay windows as defined by the signal-to-background ratio (S/B) of the dose-response TR-FRET signals. The cell lysates from the HEK293T cells expressing His-SMAD4^{WT} or SMAD4^{R361H} together with Flag-SMAD3 were serial diluted for TR-FRET assay. The data are presented as mean ± SD from a representative experiment.

(D) The waterfall plot showing the change of TR-FRET signal (ΔTR-FRET) induced by compounds from the primary screening. The data are presented as the percentage of the DMSO control from the primary screening.

(E) Chemical structures of two highly ranked SMAD4^{R361H}/SMAD3 PPI inducers, Ro-31-8220 and Go-6983.

(F and G) Dose-dependent curves of (F) Ro-31-8220 and (G) Go-6983 in enhancing the TR-FRET signal of the SMAD4^{R361H}/SMAD3 PPI. The data are presented as mean ± SD from three independent experiments.

transfer (TR-FRET) assay in a 1,536-well plate-based ultra-high-throughput screening (uHTS) format and the identification of compounds that can induce the interaction of mutated SMAD4 with SMAD3. From a bioactive compound library, we identified Ro-31-8220 and Go-6983, bisindolylmaleimide derivatives, as small-molecule inducers that restored SMAD4^{R361H} PPI with SMAD3 and revitalized the TGF-β-induced anti-proliferation function in colon cancer cell lines with SMAD4 mutations.

RESULTS

Design and development of the TR-FRET assay for SMAD4/SMAD3 PPI

To enable the unbiased systematic discovery of small-molecule PPI inducers, a sensitive and scalable high-throughput technology platform is essential to monitor the differential PPI status between SMAD3 and SMAD4 WT or R361H. Toward this goal, we examined the feasibility of the TR-FRET technology and tested it in a miniaturized 1,536-well plate format. Using the known SMAD4-SMAD3 PPI as a positive control, we have optimized the TR-FRET assay using cell lysates that co-expressed His-SMAD4 and Flag-SMAD3, and the coupled fluorophore pair anti-flag-Tb (donor) and anti-His-D2 (acceptor). The direct SMAD4-SMAD3 PPI brings Tb and D2 fluorophores into close

proximity that allows efficient energy transfer, generating TR-FRET signals (Figure 1A). In support of this design, we observed that the cell lysate containing His-SMAD4 and Flag-SMAD3 exhibited significantly higher TR-FRET signals than the corresponding empty vector controls in a concentration-dependent manner (Figure 1B). These results suggested the feasibility of using this FRET donor/acceptor configuration to monitor the SMAD4-SMAD3 PPI. The use of the cell lysates with expressed SMAD proteins eliminates the need for labor-intensive protein purification and has the benefit of the complex cellular environment (Li et al., 2017).

To evaluate the sensitivity needed to capture a single amino acid change-induced difference of the SMAD4-SMAD3 PPI dynamics, we compared the PPI signals between SMAD4 WT and R361H mutant with SMAD3. With the same configuration of protein tags and fluorophore-conjugated antibody pairs, SMAD4^{R361H} exhibited drastically decreased TR-FRET signals, showing a significant differential assay window along with the WT SMAD4 PPI (signal-to-background ratio of 10-fold versus 30-fold) (Figure 1C). Our results confirmed the importance of R361 residue of SMAD4 in heteromeric SMAD4/SMAD3 complex formation, and most importantly demonstrated the high sensitivity of the TR-FRET assay in monitoring the differential PPI dynamics at single-amino acid resolution.

TR-FRET screening reveals potential PPI inducers for mutant SMAD4

To examine the utility of this TR-FRET assay to identify small-molecule PPI inducers that can restore mutant SMAD4 interaction with SMAD3, we screened the Emory Enriched Bioactive Library (EEBL), a library of 2,036 bioactive compounds, including FDA-approved drugs and defined bioactive compounds (Mo et al., 2019). For the primary screening, we utilized the His-SMAD4^{R361H}/Flag-SMAD3 pair. To maximize the opportunity to reveal inducers that can enhance mutant SMAD4/SMAD3 interaction, the EC$_{90}$ (90% maximal effective concentration) condition of the SMAD4^{R361H}/SMAD3 interaction was selected, which corresponded to EC$_{10}$ (10% maximal effective concentration) of the WT SMAD4/SMAD3 PPI. This selection was based on our assessment of the assay performance, such as assay window between WT and R361H, DMSO tolerance, and robustness in the 1,536-well plate uHTS format (Figure S1).

Using the established condition, we performed the primary screening by treating the cell lysate co-expressing His-SMAD4^{R361H} and Flag-SMAD3 with the EEBL compounds (20 μM). Based on the potentiation effect of >40% compared with the DMSO control, the top ranked 23 primary hits were cherry-picked from the parental stock for dose-response studies (Figure 1D). Through the dose-response confirmatory assay with cherry-picked and re-ordered compounds, 8 out of 23 primary hits were validated with significant and reproducible effect in increasing the TR-FRET signal of SMAD4^{R361H}-SMAD3 PPI. The other primary hits were triaged due to their low potency or lack of consistent effect.

Identification of Ro-31-8220 and Go-6983 as SMAD4^{R361H}-SMAD3 PPI inducers

Among positive hit compounds, Ro-31-8220 and Go-6983 (Figure 1E), two bisindolylmaleimide compounds, showed robust potentiation effect of >40% for the SMAD4^{R361H}-SMAD3 PPI from the primary screening. Ro-31-8220 and Go-6983 induced the increase of the TR-FRET signal in a dose-dependent manner with half maximal effective concentration (EC$_{50}$) of 3.9 ± 1.0 and 15.2 ± 2.9 μM, respectively (Figures 1F and 1G). These data confirmed their activity in promoting the SMAD4^{R361H}-SMAD3 interaction, demonstrating the utility of the TR-FRET assay for systematic discovery of PPI inducers.

To further validate the PPI stabilization effect of these two compounds in orthogonal assays, we tested whether they can restore SMAD4^{R361H}-SMAD3 complex formation using an affinity-based GST beads pull-down assay. In the GST pull-down assay, a substantial amount of SMAD3 was detected in complex with GST-SMAD4^{WT}, whereas the R361H mutation of SMAD4 significantly decreased SMAD3 in the complex, as reported previously (Figure 2A) (Blackford et al., 2009; Fleming et al., 2013; Salovaara et al., 2002). Upon treatment of the cell lysate with Ro-31-8220, the amount of SMAD3 in the SMAD4^{R361H} complex was significantly increased in a dose-dependent manner, with an EC$_{50}$ of 2.1 ± 0.7 μM (Figure 2A). Similarly, Go-6983 enhanced the complex formation between SMAD3 and SMAD4^{R361H} with an EC$_{50}$ of 8.9 ± 0.7 μM (Figure 2B). These data support the potential stabilization effect of Ro-31-8220 and Go-6983 in enhancing the SMAD4^{R361H}-SMAD3 interaction. To evaluate the mutation selectivity of Ro-31-8220 and Go-6983, we exam-

ined their potentiation effect on other SMAD4 loss-of-function mutations, such as D351H (Fleming et al., 2013). The PPI between SMAD3 and SMAD4^{D351H} was studied in the presence of these compounds with DMSO as a control. Similarly, D351H impairs SMAD4-SMAD3 PPI complex formation, and treatment with Ro-31-8220 and Go-6983 significantly restored the SMAD3 level in the SMAD3^{D351H} GST pull-down complex (Figure 2C). Altogether, the results suggest that these compounds can enhance the interaction between both D351H and R361H with SMAD4 and SMAD3. These data imply that reduced interaction with SMAD4 by selected mutant SMAD4 may be due to a shared mechanism.

SMAD4 loss-of-function mutations not only impair its PPI with SMAD3 but also with other receptor-regulated SMADs (R-SMADs), such as SMAD1, SMAD2, SMAD5, and SMAD8 (Guo and Wang, 2009; Retting et al., 2009; Wu et al., 2016). To determine the R-SMADs selectivity of Ro-31-8220 and Go-6983, we profiled their effects on inducing PPI between SMAD4^{R361H} and different isoforms of R-SMADs using the TR-FRET assay. With the compound titration, we found that Ro-31-8220-induced increase of the TR-FRET signal is significantly higher for the SMAD4^{R361H} interaction with SMAD3 than that with other R-SMADs (Figure 2D). Similarly, Go-6983 induced a significantly higher PPI signal for SMAD4^{R361H} interaction with SMAD3 as compared with other R-SMADs (Figure 2E). Among these R-SMADs, SMAD3 and SMAD2, which mediate TGF-β signaling, appeared to have significantly higher compound-induced TR-FRET signals than SMAD1, SMAD5, and SMAD8, which mediate bone morphogenetic protein (BMP) signaling (Figures 2D and 2E). These data suggest that, among all the tested R-SMADs, Ro-31-8220 and Go-6983 are selective in inducing the interaction of SMAD4^{R361H} with SMAD3 and SMAD2.

The bisindolylmaleimides, Ro-31-8220 and Go-6983, are structurally similar staurosporine analogs with a reported activity as ATP-competitive inhibitors of protein kinase C (PKC) (Davis et al., 1989). Given the in vitro cell lysate conditions used for the identification of Ro-31-8220 and Go-6983 as SMAD4^{R361H}-SMAD3 PPI inducers, we tested whether such PPI stabilization effects are due to their PKC inhibitory activity. We selected a panel of PKC inhibitors, including five bisindolylmaleimide derivatives and two structurally diverse PKC inhibitors, and tested their activities in enhancing the SMAD4^{R361H}-SMAD3 PPI. From the dose-response study using the TR-FRET assay, all the bisindolylmaleimide derivatives exhibited similar PPI potentiation effects, with EC$_{50}$ values ranging from 4 to 20 μM, whereas the other two structurally diverse PKC inhibitors had no significant effect up to 100 μM (Table 1). Among these compounds, there is no significant correlation between their PPI-enhancing and PKC-inhibitory activities (Figure S2). Taken together, these results suggest that the SMAD4^{R361H}-SMAD3 PPI stabilization effect induced by Ro-31-8220 is most likely due to the bisindolylmaleimide core structure. Given that Ro-31-8220 exhibited the most potent PPI stabilization effect among the tested compounds, it was selected as an example for the subsequent characterization and functional studies.

To test the potential assay interference by protein fusions or tags in the overexpression system, the effect of Ro-31-8220 on promoting SMAD4^{R361H}-SMAD3 complex formation was
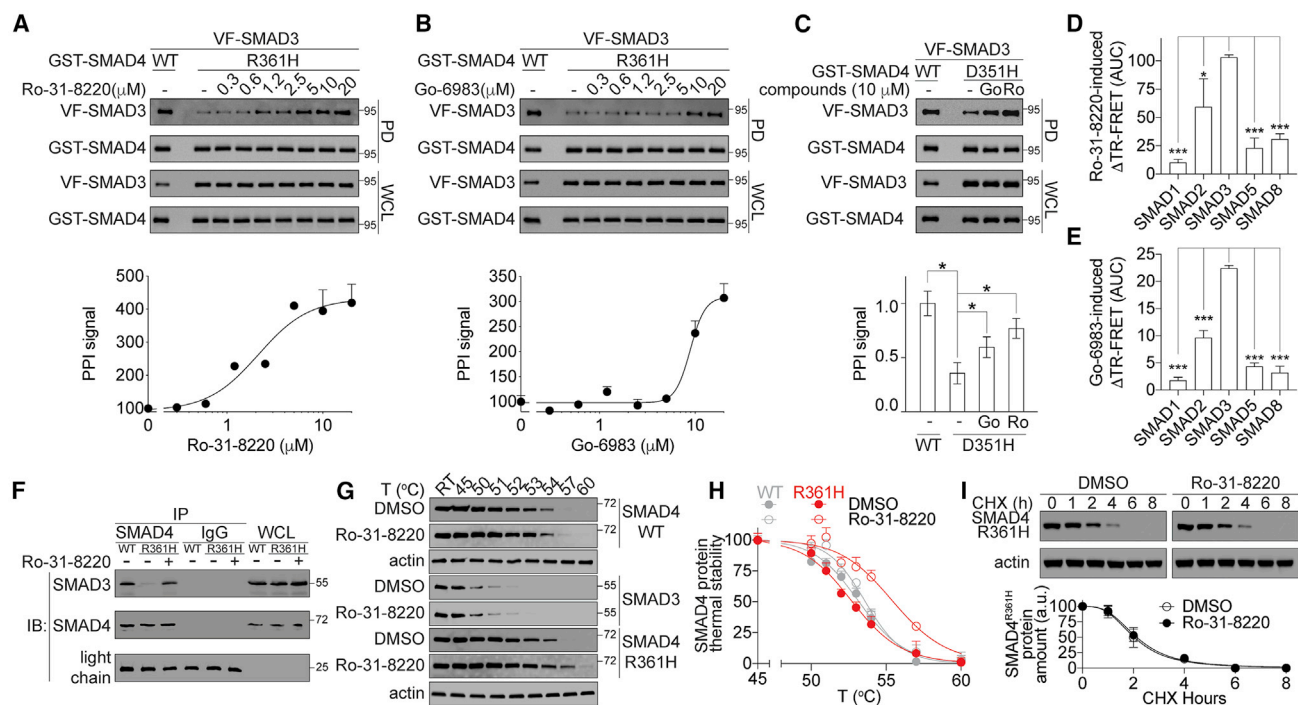
Figure 2. Validation and selectivity profiling of Ro-31-8220 as a SMAD4[R361H]/SMAD3 PPI inducer

(A and B) Western blot (upper) and dose-response curves from the gel quantification (lower) showing the induced formation of the SMAD4[R361H]/SMAD3 PPI by (A) Ro-31-8220 and (B) Go-6983. The cell lysates expressing the GST-SMAD4[R361H] and Venus-flag-tagged (VF) SMAD3 were treated with compound as indicated. Upper, the protein samples from the GST pull-down (PD) and the whole-cell lysates (WCL) were analyzed by western blotting. Lower, the dose-response curves of the PPI signal were derived from the densitometry analysis of the gels above. The data are presented as mean ± SD from three independent experiments.

(C) Western blot (upper) and the gel quantification (lower) showing the stabilization of SMAD4[D351H]/SMAD3 PPI by Ro-31-8220 and Go-6983. The cell lysates expressing the GST-SMAD4-D351H and VF-SMAD3 were treated with compounds as indicated. Upper, the protein sample from the PD and WCL were resolved by SDS-PAGE and analyzed by western blotting. Lower, the quantifications of the PPI signals from the densitometry analysis of the gels above. The data are presented as mean ± SD from three independent experiments. *$p \leq 0.05$.

(D and E) Bar graph showing the R-SMADs selectivity profiling. The cell lysates expressing Flag-SMAD3 and His-R-SMADs, including SMAD1/2/3/5/8, respectively, were treated with (D) Ro-31-8220 or (E) Go-6983 in a dose-dependent manner. The dose-response TR-FRET signal was quantified as the area under the curve (AUC). Higher AUC correlates with higher compound-induced ΔTR-FRET. The data are presented as mean ± SD from three independent experiments. *$p \leq 0.05$, ***$p \leq 0.001$.

(F) Endogenous co-immunoprecipitation validation of the Ro-31-8220's inducer effect on the SMAD4[R361H]-SMAD3 PPI. The SMAD4 PPI complex was immunoprecipitated from HCT116 (WT) or RCM-1 (R361H) cells and analyzed by immunoblotting as indicated.
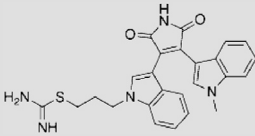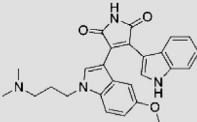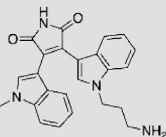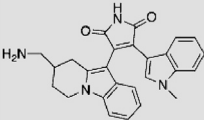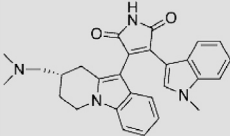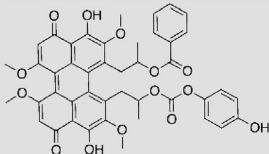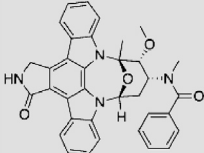
(G and H) Western blot (G) and thermal stability curves from the gel quantification (H) showing the thermal stability of SMAD4 WT or R361H in the presence of Ro-31-8220. The HCT116 (SMAD4[WT]) and RCM-1 (SMAD4[R361H]) were treated with 10 μM Ro-31-8220 for 8 h. The cells were then subjected to CETSA with heat treatment as indicated. The remaining soluble SMAD4 proteins were resolved by SDS-PAGE for western blotting. Actin from the WT and R361H cells with Ro-31-8220 treatment were used as loading control. The thermal stability curves were derived from the densitometry analysis of the western blot results. The data in (H) are presented as mean ± SD from three independent experiments.

(I) SMAD4[R361H] protein half-life from cycloheximide (CHX) chase assay. RCM-1 cells with endogenous SMAD4[R361H] mutation were treated with Ro-31-8220 or DMSO. Immunoblot (upper) and densitometry analysis (lower) showing SMAD4[R361H] and actin levels in RCM-1 cells at different CHX chase time points.

examined under endogenous protein expression conditions in human cancer cells. Colon cancer cell lines, HCT116 carrying SMAD4[WT] and the RCM-1-harboring R361H mutation, were used to study the PPI dynamics at their endogenous expression levels. From the co-immunoprecipitation assay, we successfully detected SMAD3 in complex with SMAD4[WT] in HCT116 cells (Figure 2F). However, the SMAD4-SMAD3 complex was significantly diminished in RCM-1 cells with the SMAD4 R361H mutation. Treatment of RCM-1 cells with Ro-31-8220 drastically restored the amount of SMAD3 in the SMAD4-R361H immunocomplex (Figure 2F). These results suggest that Ro-31-8220 can stabilize SMAD4[R361H]-SMAD3 PPI in colon cancer cells with the R361H mutation under endogenous conditions.

Direct interaction of small molecules with target proteins often leads to altered thermal stability of targets (Jafari et al., 2014; Martinez Molina et al., 2013). To determine whether Ro-31-8220 directly engages SMAD4[R361H] and/or SMAD3 for their enhanced interaction, the thermal stability of SMAD proteins was evaluated upon compound treatment. Colon cancer cell lines HCT116 and RCM-1 were used to study the SMAD protein engagement of Ro-31-8220. Using a cellular thermal shift assay (CETSA), we observed that both SMAD4 WT and R361H proteins exhibited temperature-dependent denaturation with similar melting temperatures (T_m) of 53.4°C ± 0.3°C and 52.7°C ± 0.3°C, respectively (Figures 2G and 2H). Upon Ro-31-8220 treatment, SMAD4

Table 1. PKC inhibitors and their activities

Compound	Chemical structure	IC$_{50}$ (PKCα) (nM)	EC$_{50}$[a] (SMAD4^{R361H}-SMAD3 PPI) (µM)
Ro-31-8220		5 (Wilkinson et al., 1993)	3.9 ± 1.0
Go-6983		7 (Gschwendt et al., 1996)	15.2 ± 2.9
Ro-31-7549		53 (Wilkinson et al., 1993)	13.0 ± 4.3
Ro-31-8425		8 (Wilkinson et al., 1993)	9.0 ± 1.7
Ro-32-0432		9 (Wilkinson et al., 1993)	19.9 ± 5.9
UCN-1028c		50 (Kobayashi et al., 1989)	>100
PKC-412		22 (Fabbro et al., 2000)	>100

[a]EC$_{50}$ was derived from the TR-FRET dose-response assay.

R361H, but not WT or SMAD3, showed an increase of T$_m$ (ΔT$_m$) of 3.8°C ± 1.5°C compared with the DMSO control group (Figures 2G and 2H). These results suggest that Ro-31-8220 is able to engage and stabilize SMAD4^{R361H} and enhances its interaction with SMAD3.

SMAD4 loss-of-function mutations have been reported to result in enhanced proteasomal degradation in a β-TrCP- and GSK3-dependent manner (Demagny et al., 2014; Demagny and De Robertis, 2016; Wan et al., 2004). To further determine whether Ro-31-8220 alters mutant SMAD4 stability, we examined the SMAD4^{R361H} protein half-life upon Ro-31-8220 treatment using a cycloheximide (CHX) chase assay. In RCM-1 cells with the endogenous SMAD4^{R361H} mutant, we observed a CHX time-dependent decrease of SMAD4^{R361H} protein level with a half-life of about 2 h when treated with Ro-31-8220, which has no significant difference compared with that with the DMSO control (Figure 2I). These results suggest that Ro-31-8220-induced SMAD4^{R361H}-SMAD3 PPI is less likely due to the interference with β-TrCP- and GSK3-mediated mutant SMAD4 protein stability.
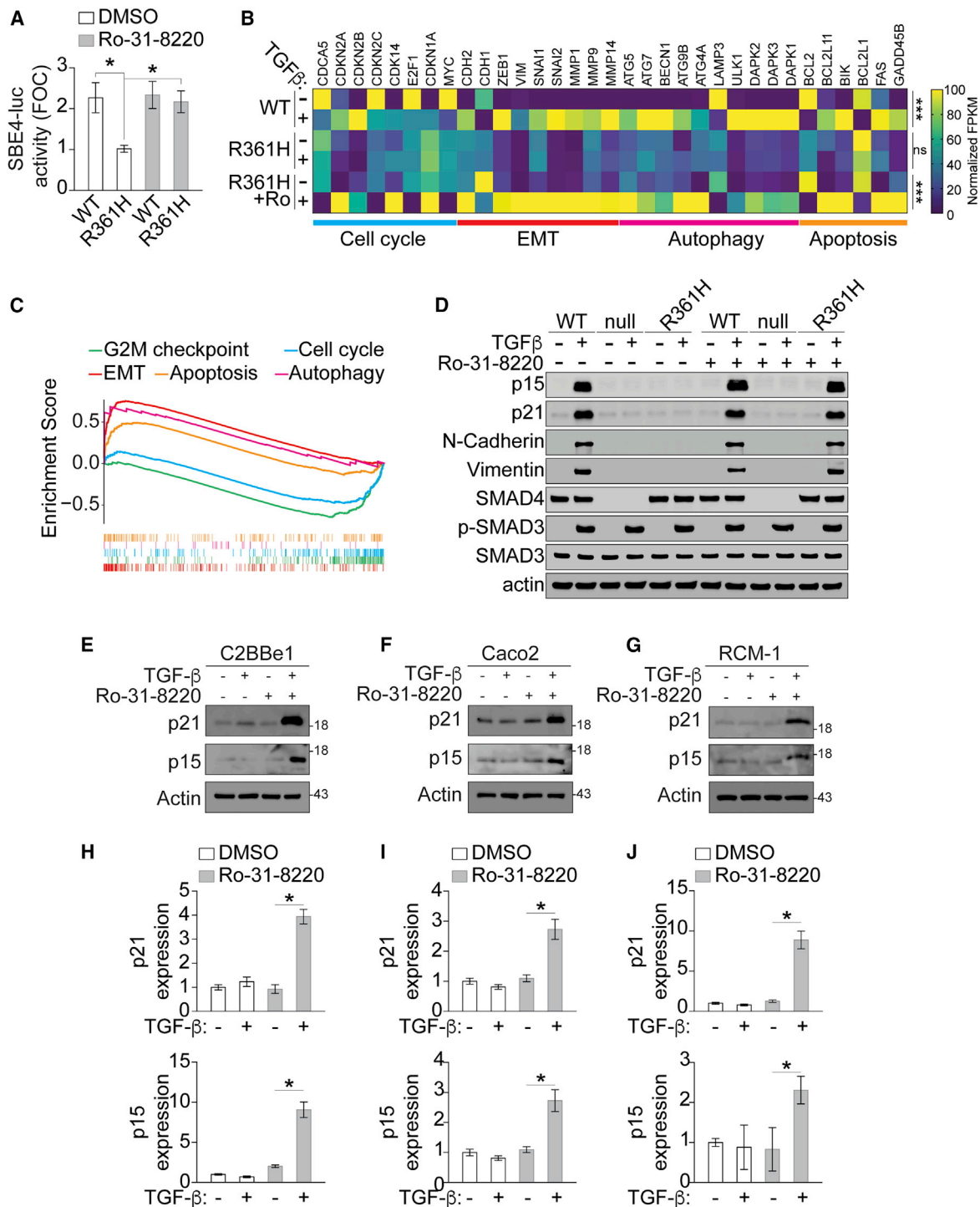
Figure 3. Ro-31-8220-induced interaction of SMAD4^mut with SMAD3 restores TGF-β signaling

(A) Ro-31-8220 restored the SMAD4/SMAD3-driven SBE-luc reporter activity. HCT116 (WT) and isogenic R361H cells were transfected with SBE-luc plasmid and treated with Ro-31-8220 or DMSO as indicated. The TGF-β-induced fold-of-change (FOC) of the luciferase signals from the WT or R361H-harboring cells are presented as mean ± SD from three independent experiments. *p ≤ 0.05.

(B) Heatmap showing differential expression genes upon TGF-β treatment. Parental HCT116 (WT) and isogenic R361H cells were treated with TGF-β (10 ng/mL) and/or Ro-31-8220 (1 μM) as indicated. The transcriptomes were analyzed by mRNA sequencing. Selected differential expression genes that are enriched in cell cycle, epithelial-to-mesenchymal transition (EMT), autophagy, and apoptosis were used to construct the heatmap. The data are presented as normalized FPKM from three technical triplicates of a single experiment. ***p ≤ 0.05, ^ns p > 0.05.

Ro-31-8220 restores TGF-β signaling in SMAD4 mutant colon cancer cells

Colon cancer cells harboring SMAD4 mutations, such as R361H, have been demonstrated to have impaired tumor-suppressive TGF-β signaling due to defects in forming the SMAD4/SMAD3 transcriptional complex (Fleming et al., 2013; Salovaara et al., 2002; Zhao et al., 2018). Since we have demonstrated that Ro-31-8220 can directly engage the mutant SMAD4 and stabilize its PPI with SMAD3, we next began to address whether Ro-31-8220-induced SMAD4^{mut}/SMAD3 PPI stabilization could functionally restore the target protein activity that is normally exhibited by the WT SMAD4/SMAD3 complex.

First, the transcriptional activity was examined as a functional readout for the SMAD4/SMAD3 complex. The SMAD4/SMAD3 transcriptional complex has been demonstrated to specifically recognize the 8-bp palindrome (Smad binding element [SBE]) sequence in the promoter region of the target genes (Zawel et al., 1998). To determine the effect of Ro-31-8220 on TGF-β signaling, we examined the fold-of-change (FOC) of the SMAD4 transcriptional activity upon TGF-β stimulation using the SBE-driven luciferase reporter assay. Colon cancer cells, parental HCT116 with WT SMAD4 and its isogenic R361H cells, were used to provide the needed SMAD4^{WT} and R361H mutation with matched genomic background. Upon TGF-β stimulation, the SMAD4^{WT} cells exhibited significant response as shown by the SBE-luc activity (FOC > 2). In contrast, the SBE-luc activity of the isogenic SMAD4 R361H cells was undetectable (FOC ∼ 1) (Figure 2A). These results confirmed the impaired transcriptional activity of the mutant SMAD4 (Fleming et al., 2013). When the isogenic R361H cells were pre-treated with Ro-31-8220, their SBE-luc activity was restored to a level similar to that of the WT cells (Figure 2A). A similar restoration effect was also observed in a patient-derived colon cancer cell line, RCM-1, which harbors the R361H mutation (Figure S3A). Thus, the Ro-31-8220-stabilized SMAD4^{R361H}/SMAD3 PPI complex appears to exhibit a gain-of-function property and can restore the lost transcriptional activity of the luciferase reporters in mutant SMAD4 cells.

To gather corroborating evidence about the effect of Ro-31-8220 on the transcription activity of mutant SMAD4, we systematically profiled the TGF-β-SMAD4/SMAD3-mediated gene expression at the transcriptome level. The parental HCT116 WT cells and their isogenic R361H cells were used to determine and compare the differentially expressed genes (DEGs) upon TGF-β treatment. For the WT cells, we observed that TGF-β-induced DEGs are significantly enriched in cell cycle, epithelial-to-mesenchymal transition (EMT), autophagy, and apoptosis pathways, which are the documented pathways and signature genes regulated by TGF-β/SMAD signaling (Figures 3B and

3C; Table S1) (Kiyon et al., 2009; Massague, 2012; Schuster and Krieglstein, 2002; Song, 2007; Xu et al., 2009; Yang et al., 2006). In contrast, no significant change or enrichment were observed for the isogenic R361H cells (Figure 3B). When the R361H cells were treated with Ro-31-8220, their response to TGF-β in terms of these DEGs was reestablished to a similar degree to that of WT cells (Figure 3B). These unbiased transcriptome profilings further suggest that Ro-31-8220 treatment leads to the regaining of R361H cell sensitivity to TGF-β, supporting the restoration of the SMAD4^{R361H}/SMAD3 PPI complex.

To validate the Ro-31-8220-induced restoration of TGF-β signaling in SMAD4 mutant cells, we next examined the protein expression of several selected DEGs from transcriptome profiling. A set of isogenic cell lines, including parental HCT116 (WT), and isogenic SMAD4 knockout (null) and R361H cells, were used to analyze the protein expression of cell-cycle regulators p15 (*CDKN2B*) and p21 (*CDKN1A*), and EMT biomarkers N-cadherin (*CDH2*) and Vimentin (*VIM*). Upon TGF-β stimulation, we observed a significant increase of p15, p21, N-cadherin, and Vimentin protein level in the WT cells, whereas no significant change was observed in the SMAD4 null and R361H cells, supporting the current loss-of-function annotation of the SMAD4 mutations in TGF-β signaling. However, when R361H mutant cells, but not SMAD4 null cells, were pre-treated with Ro-31-8220, we observed a significant increase of TGF-β-induced expression of p15, p21, N-cadherin, and Vimentin proteins. Such Ro-31-8220-induced restoration of p15 and p21 mRNA and protein expression were further confirmed in a panel of patient-derived SMAD4 mutant cell lines (Figures 3E–L and S3B–S3I). These results provided evidence at the protein level that Ro-31-8220 can restore TGF-β-triggered expression of SMAD4/SMAD3-regulated gene products in the SMAD4 mutant cells.

Ro-31-8220 restores TGF-β tumor suppression function in SMAD4 mutant colon cancer cells

Given the demonstrated capability of Ro-31-8220 in restoring the SMAD4^{mut}/SMAD3 PPI and the tumor-suppressive TGF-β signaling in the SMAD4 mutation cells, we tested whether Ro-31-8220 can promote TGF-β-evoked anti-proliferation function in cancer cells with SMAD4 missense mutations. Three functional assays were performed to measure the effect of Ro-31-8220 on cell-cycle progression, cell proliferation, and colony formation with WT and isogenic SMAD4 mutant colon cancer cells.

From flow cytometry-based cell-cycle analysis, we found that WT cells were sensitive to TGF-β, showing significantly increased number of cells in the G1/S phase, while the R361H isogenic cells were insensitive to TGF-β-induced G1/S arrest (Figure 4A), which is consistent with the cell-cycle-associated gene expression signatures. However, R361H cells treated with Ro-31-8220 regained

(C) Gene set enrichment analysis showing significant enrichment of differential expression genes from WT cells treated with TGF-β as compared with the vehicle control.

(D) Immunoblot showing the validation of Ro-31-8220-induced restoration of TGF-β signaling at protein levels. HCT116 cells (WT) and corresponding SMAD4 knockout (null) or R361H isogenic cells were treated with TGF-β (10 ng/mL) and/or Ro-31-8220 (1 μM) as indicated. Representative western blot images are presented from three independent experiments.

(E–G) Ro-31-8220 induced restoration of p21 and p15 protein levels in SMAD4 mutant cells. SMAD4 mutant cells, (E) C2BBe1 (D351H), (F) Caco2 (D351H), and (G) RCM-1 (R361H) cells, were treated with TGF-β (10 ng/mL) or in combination with Ro-31-8220 (1 μM). The protein samples from the cell lysate were analyzed by western blot. (H–J) Bar graphs showing the quantification of p21 (upper) and p15 (lower) protein through the densitometry analysis of the western blot results from the SMAD4 mutant cells, (H) C2BBe1 (D351H), (I) Caco2 (D351H), and (J) RCM-1 (R361H), as shown in (E and G). The data are presented as mean ± SD from three independent experiments. *p ≤ 0.05.
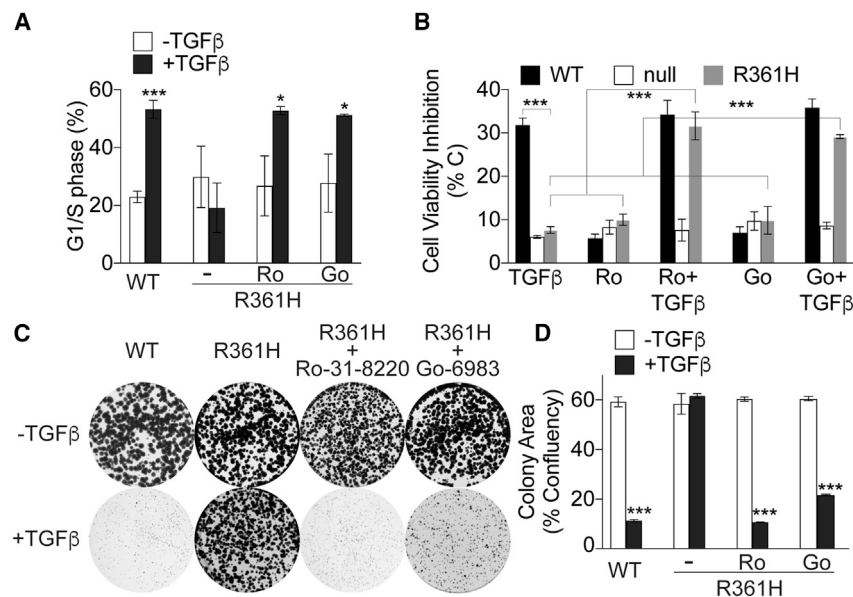
Figure 4. Ro-31-8220- and Go-6983-induced interaction of SMAD4^{mut} with SMAD3 restores TGF-β tumor suppression function

(A) Bar graphs showing the quantification of colon cancer cells in G1/S phase. Parental HCT116 (WT) and isogenic R361H cells were treated with TGF-β (10 ng/mL), Ro-31-8220 (1 μM), Go-6983 (10 μM), or in combination as indicated. The percentage of cells staying in G1/S phase was determined by flow cytometry and are presented as mean ± SD from three independent experiments. *p ≤ 0.05, ***p ≤ 0.001.

(B) Synergistic effect of TGF-β with Ro-31-8220 or Go-6983 in inhibiting cell viability in the set of isogenic HCT116 colon cancer cells. HCT116 cells (WT) and corresponding SMAD4 knockout (null) or R361H, isogenic cells were treated with TGF-β (10 ng/mL), Ro-31-8220 (1 μM), Go-6983 (10 μM), or in combination as indicated. The cell viability after treatment was measured using the CellTiter-Blue reagent and normalized to the untreated vehicle or DMSO controls (% C). The data are presented as mean ± SD of three independent experiments. ***p ≤ 0.001.

(C) Images showing the synergistic effect of TGF-β and Ro-31-8220 or Go-6983 in inhibiting colon cancer cell colony formation. Parental HCT116 (WT) and isogenic R361H cells were treated with TGF-β (10 ng/mL), Ro-31-8220 (1 μM), Go-6983 (10 μM), or in combination as indicated. Representative images are presented from three independent experiments.

(D) Bar graphs of the quantification of colony area from the colony formation assay showing the synergistic effect of TGF-β with Ro-31-8220 or Go-6983 in inhibiting colon cancer cell colony formation.

The data are presented as mean ± SD from three independent experiments. ***p ≤ 0.001.

sensitivity to TGF-β-induced G1/S cell-cycle arrest (Figure 4A). A similar re-sensitization effect was also observed with Go-6983 treatment (Figure 4A). These results support the role of Ro-31-8220 in restoring the SMAD4^{R361H}/SMAD3 PPI to transmit TGF-β-triggered signaling, resulting in expression of defined cell-cycle regulatory genes and the enhanced cell-cycle arrest.

As well as the cell-cycle regulatory genes, Ro-31-8220 treatment also restored the transcriptional response of R361H cells to TGF-β in terms of pro-apoptotic and pro-autophagy genes that may promote cell death. Thus, we examined the effect of Ro-31-8220 on TGF-β-regulated cell proliferation in the context of the SMAD4 mutation. As reported, TGF-β induced a significant decrease of cell viability of SMAD4 WT cells, while the isogenic SMAD4 null or R361H cells were resistant to such TGF-β-induced growth suppression (Figure 4B). The Ro-31-8220 treatment alone did not result in any significant growth inhibition among SMAD4 WT, null, and R361H cells (Figure 4B). However, Ro-31-8220 restored the sensitivity of SMAD4 R361H cells, but not null cells, to TGF-β-induced growth suppression, showing significantly reduced viability comparable with that of WT cells (Figure 4B). The combination of Ro-31-8220 with TGF-β exhibited a synergistic effect, showing enhanced growth inhibition of cells with SMAD4 R361H. Similar effects were also observed for Go-6983 in this set of isogenic cells, as well as in a panel of patient-derived colon cells (Figures 4B and S4A).

The lost tumor suppressor function of mutated SMAD4, R361H, can be recapitulated in an *in vitro* tumorigenic assay. As shown in Figure 4A, colon cancer HCT116 cells with WT and their isogenic mutant SMAD4 cells can grow into large colonies. This clonogenic activity of HCT116 with SMAD4^{WT} can be suppressed by TGF-β, showing diminished sizes of the colonies formed, whereas isogenic cells with SMAD4 R361H were resistant to TGF-β, retain-

ing large colonies with TGF-β treatment (Figures 4C and 4D). Upon Ro-31-8220 treatment in combination with TGF-β, the R361H cells showed significantly decreased colony area, suggesting that they regained the sensitivity to TGF-β-induced inhibition of colony formation (Figures 4C and 4D). A similar effect was also observed for Go-6983 in this pair of isogenic cell lines, as well as in other patient-derived colon cancer cells with SMAD4 mutations (Figures 4C, 4D, and S4B). Altogether, our results suggest that Ro-31-8220 and Go-6983 can synergize with TGF-β to induce the growth inhibition and clonogenic activity of colon cancer cells harboring the SMAD4 missense mutations, and such a synergistic effect depends on the presence of mutant SMAD4 proteins.

DISCUSSION

Through a uHTS approach, we have identified small-molecule glues that can enhance the interaction of the hypomorph SMAD4^{R361H} with SMAD3, leading to a restored functional complex with activity similar to that of the WT SMAD4/SMAD3 complex. Ro-31-8220 and Go-6938, SMAD4^{R361H}/SMAD3 PPI inducers, can not only enhance the physical interaction of the mutant SMAD4 with SMAD3, but can also lead to functional activation of the TGF-β-triggered transcriptional activity, and re-sensitize SMAD4^{R361H}-carrying colon cancer cells to TGF-β-induced oncogenic growth suppression. Our results support a variant-directed PPI inducer discovery approach to develop PPI functional activators to reverse the lost function of tumor suppressors.

Tumor suppressor gene-inactivating mutations are found to be major cancer drivers, or enablers, in the most common solid tumors, offering vast tumor suppressor mutation space for tumor-specific therapeutic discovery (Vogelstein et al., 2013).

However, it is a daunting task to use small molecules to intervene with such tumor suppressors, which are usually mutated, deleted, or silenced in cancer, lacking "druggable" targets. Our study illustrates the feasibility of targeting the loss-of-function tumor suppressor mutations through a variant-directed, in this case hypomorph mutation-directed, small-molecule PPI-inducer approach using the R361H missense mutation in SMAD4 as an example. Our identification of Ro-31-8220 and Go-6938 as hypomorph mutation-targeted PPI inducers suggests a powerful strategy to regain the lost growth-suppressive function caused by inactivating mutations in tumor suppressors. It is recognized that, among the undruggable tumor suppressors, the presence of a loss-of-function, or hypomorph, missense mutation residing in the intact proteins often represents a unique opportunity for the discovery of small-molecule PPI activators to restore their function, as we have shown with SMAD4^{R361H}. Our approach could be extended to a wide range of mutated tumor-suppressor proteins. Other examples of such hypomorph mutations include missense mutations in the SPOP substrate-recognition MATH domain impairing the interactions with SRC3 and BRD4 PPI (Dai et al., 2017; Geng et al., 2013; Zhuang et al., 2009), missense mutations in the KEAP1 KELCH domain disrupting the interaction with NRF2 (Li et al., 2004; Padmanabhan et al., 2006), and mutations in FBXW7 WD40 propeller domain perturbing the interaction with CCNE1 PPI (Akhoondi et al., 2007; Hao et al., 2007). Our reported variant-directed PPI activator approach could be applied to identify desired small-molecule inducers to restore the formation of their respective WT protein complexes for functional and therapeutic studies.

A number of natural products and synthetic compounds have been found to induce protein-protein interactions with demonstrated clinical applications, such as cyclosporine and rapamycin (Andrei et al., 2017; Benjamin et al., 2011; Choi et al., 1996; Gerry and Schreiber, 2020; Liu et al., 1991). Synthetic compounds have been identified to bridge and stabilize protein-protein interactions, such as 14-3-3-mediated interactions (Andrei et al., 2018; Andrei et al., 2017; Fu et al., 2000; Gigante et al., 2020; Sijbesma et al., 2019). These small-molecule-induced protein-protein interactions often lead to functional inhibition of their binding targets. Rapamycin inhibits mTOR signaling while taxol-stabilized tubulins inhibit microtubule dynamics and cell-cycle arrest (Liu et al., 1991; Schiff and Horwitz, 1980). The synthetic PROTAC probes are designed to recruit and stabilize the PPI ubiquitination complex, leading to the degradation of targeted substrates (Lai and Crews, 2017). A unique feature of the current work is that the Ro-31-8220 PPI inducer promotes SMAD4^{R361H}/SMAD3 complex formation, and reverts the complex to its WT active PPI function, leading to its subsequent transcriptional activation and tumor-suppressive signaling. The missense mutation-oriented small-molecule activator function adds a critical advantage for tumor-selective targeting and genomics-based therapeutic discovery.

The bisindolylmaleimide, Ro-31-8220, identified from our study has been initially reported to be a selective PKC inhibitor (Davis et al., 1989). In addition to inhibiting PKC, Ro-31-8220 was later found to inhibit mitogen-activated protein kinase phosphatase-1 expression, induce c-Jun expression, and activate Jun N-terminal kinase, in a PKC-independent manner (Beltman et al., 1996). Our data suggest that Ro-31-8220 has additional pharmacological properties in stabilization of the SMAD4^{MUT}/SMAD3 PPI, which are correlated with the bisindolylmaleimide structure but not PKC inhibition activity. The PKC-independent activity of Ro-31-8220 in PPI stabilization was further supported by our observation that Ro-31-8220 can restore p21 expression induced by TGF-β, which is in contrast to the reported activity of Ro-31-8220 in PKC inhibition, resulting in PKC-regulated p21 downregulation (Park et al., 2001). The crosstalk between PKC and TGF-β signaling has been reported. PKC-mediated phosphorylation of SMAD3 impairs its DNA binding and thus downregulates the growth inhibition induced by TGF-β (Yakymovych et al., 2001). However, such PKC-SMAD3 connectivity could not explain our observation of the differential effect of Ro-31-8220 in regulating the TGF-β signaling between WT and mutant SMAD4 colon cancer cells with the same SMAD3 genetic status, further suggesting the likelihood of an underlying PKC-independent activity of Ro-31-8220.

SMAD4 is a common SMAD that cooperates with various R-SMADs in diverse signaling pathways. Ro-31-8220 was identified from a uHTS that was specifically designed to reveal PPI inducers for the SMAD4^{R361H} interaction with SMAD3. Indeed, from our R-SMAD profiling studies, Ro-31-8220 showed preferential interactions of SMAD4^{R361H} with SMAD3 and SMAD2, R-SMADs involved in TGF-β-signaling, to that of SMAD1, SMAD5, or SMAD8, mediators of BMP signaling (Figure 2D). This selectivity is likely due to structural differences between the SMAD2/3 subclass and the SMAD1/5/8 subclass (Macias et al., 2015; Miyazono et al., 2018). The structural determinants in SMAD2/3 that are critical for their interaction with mutated SMAD4 bridged by Ro-31-8220 may not be conserved in SMAD1/5/8. Such a selectivity may allow the use of Ro-31-8220-type PPI inducers to address SMAD4^{R361H}-dependent TGF-β signaling.

TGF-β has demonstrated paradoxical activities in cancer: a tumor-suppressive role in pre-malignant cells and an enhancing role for invasion and metastasis in late-stage cancers (Massague, 2008). Oncogenic mutations are often selected to overcome TGF-β tumor-suppressive activity for tumorigenesis and progression. For example, inactivation mutations in SMAD4 recurrent in colon and pancreatic tumors can counter the TGF-β action, showing enhanced clonogenic activity that is resistant to TGF-β (Figure 4) (Massague, 2008; Papageorgis et al., 2011). Here, we show that Ro-31-8220 not only induces the SMAD4^{R361H} interaction with SMAD3, but also restores the responsiveness of SMAD4^{R361H}-carrying colon cancer cells to TGF-β signaling and its clonogenic suppression activity (Figure 4), supporting a potential anticancer role of Ro-31-8220 in these tumors. Our transcriptome data further showed that TGF-β induced the DEGs involved in both anti-proliferative and pro-EMT pathways in a SMAD4^{WT}-dependent manner in these cell lines, whereas Ro-31-8220 can restore the transcriptome responsiveness of SMAD4^{R361H} cells to TGF-β (Figure 3B). These results demonstrate an important role of Ro-31-8220 in the regulation of the TGF-β-triggered molecular programs. How Ro-31-8220 modulates the SMAD4^{R361H}-mediated proliferative activity, and/or possible tumor progression activity, may be dependent on the cellular states, the stages of cancer development, and the type of tumors with particular vulnerabilities, which

warrants further studies (Massague, 2008; Song, 2007; Song and Shi, 2018). Together, these data support the development of the Ro-31-8220 class of chemical probes to decipher the role of the SMAD4^{R361H}/SMAD3 node in TGF-β signaling and in cancer biology for precision medicine.

Our identification of bisindolylmaleimides, such as Ro-31-8220 and Go-6938, as SMAD4^{MUT}/SMAD3 PPI inducers strongly supports the systematic strategy of target-based discovery of PPI activators through *de-novo*-unbiased HTS campaign. These bisindolylmaleimides represent the first-in-class SMAD4^{MUT}/SMAD3 PPI inducers identified from the HTS campaign. It may serve as a promising chemical scaffold to develop clinical candidates for the treatment of patients with SMAD4^{MUT}-carrying cancers, such as pancreatic, colon, and skin cancers.

SIGNIFICANCE

We have developed a uHTS TR-FRET platform to monitor the differential interaction of WT and mutant SMAD4 with SMAD3 at single-amino acid resolution, which was used to discover small-molecule PPI inducers that can restore the PPI formation between SMAD4^{R361H} and SMAD3. The identification of the derivatives of bisindolylmaleimides, such as Ro-31-8220, which induces SMAD4^{MUT}/SMAD3 PPI and re-establishes tumor-suppressive TGF-β signaling, supports the feasibility of using *de novo* screening for small-molecule PPI molecular glue discovery. Similar strategies could be readily adapted to a wide range of other loss-of-function missense mutations for identification of hypomorph mutation-specific molecular glues, which could be expanded to discover PROTAC-like probes for promoting the artificial PPI complex for therapeutic intervention. Importantly, Ro-31-8220 represents a hypomorph mutation-directed small-molecule PPI inducer and activator, which can be used to functionally reestablish the suppressed function of the mutant protein-protein interactions. Such small-molecule activators may be developed as potential therapeutic agents to restore the tumor suppression function of WT proteins for cancer therapy, allowing the scope to reach the vast un-drugged mutated tumor suppressor target space.

STAR★METHODS

Detailed methods are provided in the online version of this paper and include the following:

- KEY RESOURCES TABLE
- RESOURCE AVAILABILITY
    - Lead contact
    - Materials availability
    - Data and code availability
- EXPERIMENTAL MODEL AND SUBJECT DETAILS
- METHOD DETAILS
    - Molecular cloning and mutagenesis
    - Time-resolved fluorescence resonance energy transfer (TR-FRET) assay
    - uHTS TR-FRET screening for small molecule PPI inducer discovery
    - GST pull-down assay
    - Co-immunoprecipitation (co-IP) with endogenous proteins
    - Cellular thermal shift assay (CETSA)
    - Protein stability assay
    - Western blot
    - SMAD binding element (SBE) luciferase reporter assay
    - Transcriptome analysis and quantitative polymerase chain reaction (qPCR)
    - Gene set enrichment analyses (GSEA)
    - Cell cycle analysis
    - Colony formation assay
    - Cell viability assay
- QUANTIFICATION AND STATISTICAL ANALYSIS

REFERENCES

Akhoondi, S., Sun, D., von der Lehr, N., Apostolidou, S., Klotz, K., Maljukova, A., Cepeda, D., Fiegl, H., Dafou, D., Marth, C., et al. (2007). FBXW7/hCDC4 is a general tumor suppressor in human cancer. Cancer Res *67*, 9006–9012.

Andrei, S.A., de Vink, P., Sijbesma, E., Han, L., Brunsveld, L., Kato, N., Ottmann, C., and Higuchi, Y. (2018). Rationally designed semisynthetic natural product analogues for stabilization of 14-3-3 protein-protein interactions. Angew. Chem. Int. Ed. *57*, 13470–13474.

Andrei, S.A., Sijbesma, E., Hann, M., Davis, J., O'Mahony, G., Perry, M.W.D., Karawajczyk, A., Eickhoff, J., Brunsveld, L., Doveston, R.G., et al. (2017). Stabilization of protein-protein interactions in drug discovery. Expert Opin. Drug Discov. *12*, 925–940.

Beltman, J., McCormick, F., and Cook, S.J. (1996). The selective protein kinase C inhibitor, Ro-31-8220, inhibits mitogen-activated protein kinase phosphatase-1 (MKP-1) expression, induces c-Jun expression, and activates Jun N-terminal kinase. J. Biol. Chem. *271*, 27018–27024.

Benjamin, D., Colombi, M., Moroni, C., and Hall, M.N. (2011). Rapamycin passes the torch: a new generation of mTOR inhibitors. Nat. Rev. Drug Discov. 10, 868–880.

Blackford, A., Serrano, O.K., Wolfgang, C.L., Parmigiani, G., Jones, S., Zhang, X., Parsons, D.W., Lin, J.C., Leary, R.J., Eshleman, J.R., et al. (2009). SMAD4 gene mutations are associated with poor prognosis in pancreatic cancer. Clin. Cancer Res. 15, 4674–4679.

Chacko, B.M., Qin, B.Y., Tiwari, A., Shi, G., Lam, S., Hayward, L.J., De Caestecker, M., and Lin, K. (2004). Structural basis of heteromeric smad protein assembly in TGF-beta signaling. Mol. Cell 15, 813–823.

Choi, J., Chen, J., Schreiber, S.L., and Clardy, J. (1996). Structure of the FKBP12-rapamycin complex interacting with the binding domain of human FRAP. Science 273, 239–242.

Dai, X., Gan, W., Li, X., Wang, S., Zhang, W., Huang, L., Liu, S., Zhong, Q., Guo, J., Zhang, J., et al. (2017). Prostate cancer-associated SPOP mutations confer resistance to BET inhibitors through stabilization of BRD4. Nat. Med. 23, 1063–1071.

Davis, P.D., Hill, C.H., Keech, E., Lawton, G., Nixon, J.S., Sedgwick, A.D., Wadsworth, J., Westmacott, D., and Wilkinson, S.E. (1989). Potent selective inhibitors of protein kinase C. FEBS Lett. 259, 61–63.

Demagny, H., Araki, T., and De Robertis, E.M. (2014). The tumor suppressor Smad4/DPC4 is regulated by phosphorylations that integrate FGF, Wnt, and TGF-beta signaling. Cell Rep. 9, 688–700.

Demagny, H., and De Robertis, E.M. (2016). Point mutations in the tumor suppressor Smad4/DPC4 enhance its phosphorylation by GSK3 and reversibly inactivate TGF-beta signaling. Mol. Cell Oncol. 3, e1025181.

Fabbro, D., Ruetz, S., Bodis, S., Pruschy, M., Csermak, K., Man, A., Campochiaro, P., Wood, J., O'Reilly, T., and Meyer, T. (2000). PKC412 — a protein kinase inhibitor with a broad therapeutic potential. Anticancer Drug Des. 15, 17–28.

Fleming, N.I., Jorissen, R.N., Mouradov, D., Christie, M., Sakthianandeswaren, A., Palmieri, M., Day, F., Li, S., Tsui, C., Lipton, L., et al. (2013). SMAD2, SMAD3 and SMAD4 mutations in colorectal cancer. Cancer Res. 73, 725–735.

Fu, H., Subramanian, R.R., and Masters, S.C. (2000). 14-3-3 proteins: structure, function, and regulation. Annu. Rev. Pharmacol. Toxicol. 40, 617–647.

Geng, C., He, B., Xu, L., Barbieri, C.E., Eedunuri, V.K., Chew, S.A., Zimmermann, M., Bond, R., Shou, J., Li, C., et al. (2013). Prostate cancer-associated mutations in speckle-type POZ protein (SPOP) regulate steroid receptor coactivator 3 protein turnover. Proc. Natl. Acad. Sci. U S A 110, 6997–7002.

Gerry, C.J., and Schreiber, S.L. (2020). Unifying principles of bifunctional, proximity-inducing small molecules. Nat. Chem. Biol. 16, 369–378.

Gigante, A., Sijbesma, E., Sanchez-Murcia, P.A., Hu, X., Bier, D., Backer, S., Knauer, S., Gago, F., Ottmann, C., and Schmuck, C. (2020). A supramolecular stabilizer of the 14-3-3zeta/ERalpha protein-protein interaction with a synergistic mode of action. Angew. Chem. Int. Ed. 59, 5284–5287.

Gschwendt, M., Dieterich, S., Rennecke, J., Kittstein, W., Mueller, H.J., and Johannes, F.J. (1996). Inhibition of protein kinase C mu by various inhibitors. Differentiation from protein kinase c isoenzymes. FEBS Lett. 392, 77–80.

Guo, X., and Wang, X.F. (2009). Signaling cross-talk between TGF-beta/BMP and other pathways. Cell Res. 19, 71–88.

Guo, X.E., Ngo, B., Modrek, A.S., and Lee, W.H. (2014). Targeting tumor suppressor networks for cancer therapeutics. Curr. Drug Targets 15, 2–16.

Guzman, C., Bagga, M., Kaur, A., Westermarck, J., and Abankwa, D. (2014). ColonyArea: an ImageJ plugin to automatically quantify colony formation in clonogenic assays. PLoS One 9, e92444.

Hao, B., Oehlmann, S., Sowa, M.E., Harper, J.W., and Pavletich, N.P. (2007). Structure of a Fbw7-Skp1-cyclin E complex: multisite-phosphorylated substrate recognition by SCF ubiquitin ligases. Mol. Cell 26, 131–143.

Jafari, R., Almqvist, H., Axelsson, H., Ignatushchenko, M., Lundback, T., Nordlund, P., and Martinez Molina, D. (2014). The cellular thermal shift assay for evaluating drug target interactions in cells. Nat. Protoc. 9, 2100–2122.

Kiyono, K., Suzuki, H.I., Matsuyama, H., Morishita, Y., Komuro, A., Kano, M.R., Sugimoto, K., and Miyazono, K. (2009). Autophagy is activated by TGF-beta and potentiates TGF-beta-mediated growth inhibition in human hepatocellular carcinoma cells. Cancer Res. 69, 8844–8852.

Kobayashi, E., Nakano, H., Morimoto, M., and Tamaoki, T. (1989). Calphostin C (UCN-1028C), a novel microbial compound, is a highly potent and specific inhibitor of protein kinase C. Biochem. Biophys. Res. Commun. 159, 548–553.

Lai, A.C., and Crews, C.M. (2017). Induced protein degradation: an emerging drug discovery paradigm. Nat. Rev. Drug Discov. 16, 101–114.

Li, X., Zhang, D., Hannink, M., and Beamer, L.J. (2004). Crystal structure of the Kelch domain of human Keap1. J. Biol. Chem. 279, 54750–54758.

Li, Z., Ivanov, A.A., Su, R., Gonzalez-Pecchi, V., Qi, Q., Liu, S., Webber, P., McMillan, E., Rusnak, L., Pham, C., et al. (2017). The OncoPPi network of cancer-focused protein-protein interactions to inform biological insights and therapeutic strategies. Nat. Commun. 8, 14356.

Liu, J., Farmer, J.D., Jr., Lane, W.S., Friedman, J., Weissman, I., and Schreiber, S.L. (1991). Calcineurin is a common target of cyclophilin-cyclosporin A and FKBP-FK506 complexes. Cell 66, 807–815.

MacGrogan, D., Pegram, M., Slamon, D., and Bookstein, R. (1997). Comparative mutational analysis of DPC4 (Smad4) in prostatic and colorectal carcinomas. Oncogene 15, 1111–1114.

Macias, M.J., Martin-Malpartida, P., and Massague, J. (2015). Structural determinants of Smad function in TGF-beta signaling. Trends Biochem. Sci. 40, 296–308.

Martinez Molina, D., Jafari, R., Ignatushchenko, M., Seki, T., Larsson, E.A., Dan, C., Sreekumar, L., Cao, Y., and Nordlund, P. (2013). Monitoring drug target engagement in cells and tissues using the cellular thermal shift assay. Science 341, 84–87.

Massague, J. (2008). TGFbeta in cancer. Cell 134, 215–230.

Massague, J. (2012). TGFbeta signalling in context. Nat. Rev. Mol. Cell Biol. 13, 616–630.

Miyaki, M., and Kuroki, T. (2003). Role of Smad4 (DPC4) inactivation in human cancer. Biochem. Biophys. Res. Commun. 306, 799–804.

Miyazono, K.I., Ohno, Y., Wada, H., Ito, T., Fukatsu, Y., Kurisaki, A., Asashima, M., and Tanokura, M. (2018). Structural basis for receptor-regulated SMAD recognition by MAN1. Nucleic Acids Res. 46, 12139–12153.

Mo, X., Tang, C., Niu, Q., Ma, T., Du, Y., and Fu, H. (2019). HTiP: high-throughput immunomodulator phenotypic screening platform to reveal IAP antagonists as anti-cancer immune enhancers. Cell Chem. Biol. 26, 331–339 e333.

Nakao, A., Imamura, T., Souchelnytskyi, S., Kawabata, M., Ishisaki, A., Oeda, E., Tamaki, K., Hanai, J., Heldin, C.H., Miyazono, K., et al. (1997). TGF-beta receptor-mediated signalling through Smad2, Smad3 and Smad4. EMBO J. 16, 5353–5362.

Padmanabhan, B., Tong, K.I., Ohta, T., Nakamura, Y., Scharlock, M., Ohtsuji, M., Kang, M.I., Kobayashi, A., Yokoyama, S., and Yamamoto, M. (2006). Structural basis for defects of Keap1 activity provoked by its point mutations in lung cancer. Mol. Cell 21, 689–700.

Papageorgis, P., Cheng, K., Ozturk, S., Gong, Y., Lambert, A.W., Abdolmaleky, H.M., Zhou, J.R., and Thiagalingam, S. (2011). Smad4 inactivation promotes malignancy and drug resistance of colon cancer. Cancer Res. 71, 998–1008.

Park, J.W., Jang, M.A., Lee, Y.H., Passaniti, A., and Kwon, T.K. (2001). p53-independent elevation of p21 expression by PMA results from PKC-mediated mRNA stabilization. Biochem. Biophys. Res. Commun. 280, 244–248.

Retting, K.N., Song, B., Yoon, B.S., and Lyons, K.M. (2009). BMP canonical Smad signaling through Smad1 and Smad5 is required for endochondral bone formation. Development 136, 1093–1104.

Salovaara, R., Roth, S., Loukola, A., Launonen, V., Sistonen, P., Avizienyte, E., Kristo, P., Jarvinen, H., Souchelnytskyi, S., Sarlomo-Rikala, M., et al. (2002). Frequent loss of SMAD4/DPC4 protein in colorectal cancers. Gut 51, 56–59.

Schiff, P.B., and Horwitz, S.B. (1980). Taxol stabilizes microtubules in mouse fibroblast cells. Proc. Natl. Acad. Sci. U S A 77, 1561–1565.

Schuster, N., and Krieglstein, K. (2002). Mechanisms of TGF-beta-mediated apoptosis. Cell Tissue Res. 307, 1–14.

Sijbesma, E., Hallenbeck, K.K., Leysen, S., de Vink, P.J., Skóra, L., Jahnke, W., Brunsveld, L., Arkin, M.R., and Ottmann, C. (2019). Site-directed fragment-based screening for the discovery of protein–protein interaction stabilizers. J. Am. Chem. Soc. *141*, 3524–3531.

Song, J. (2007). EMT or apoptosis: a decision for TGF-beta. Cell Res. *17*, 289–290.

Song, J., and Shi, W. (2018). The concomitant apoptosis and EMT underlie the fundamental functions of TGF-beta. Acta Biochim. Biophys. Sin (Shanghai) *50*, 91–97.

Sun, S.Y., Rosenberg, L.M., Wang, X., Zhou, Z., Yue, P., Fu, H., and Khuri, F.R. (2005). Activation of Akt and eIF4E survival pathways by rapamycin-mediated mammalian target of rapamycin inhibition. Cancer Res. *65*, 7052–7058.

Vogelstein, B., Papadopoulos, N., Velculescu, V.E., Zhou, S., Diaz, L.A., Jr., and Kinzler, K.W. (2013). Cancer genome landscapes. Science *339*, 1546–1558.

Wan, M., Tang, Y., Tytler, E.M., Lu, C., Jin, B., Vickers, S.M., Yang, L., Shi, X., and Cao, X. (2004). Smad4 protein stability is regulated by ubiquitin ligase SCF beta-TrCP1. J. Biol. Chem. *279*, 14484–14487.

Wilkinson, S.E., Parker, P.J., and Nixon, J.S. (1993). Isoenzyme specificity of bisindolylmaleimides, selective inhibitors of protein kinase C. Biochem. J. *294* (Pt 2), 335–337.

Woodford-Richens, K.L., Rowan, A.J., Gorman, P., Halford, S., Bicknell, D.C., Wasan, H.S., Roylance, R.R., Bodmer, W.F., and Tomlinson, I.P. (2001). SMAD4 mutations in colorectal cancer probably occur before chromosomal instability, but after divergence of the microsatellite instability pathway. Proc. Natl. Acad. Sci. U S A *98*, 9719–9723.

Wu, M., Chen, G., and Li, Y.P. (2016). TGF-beta and BMP signaling in osteo-blast, skeletal development, and bone formation, homeostasis and disease. Bone Res. *4*, 16009.

Xu, J., Lamouille, S., and Derynck, R. (2009). TGF-beta-induced epithelial to mesenchymal transition. Cell Res. *19*, 156–172.

Yakymovych, I., Ten Dijke, P., Heldin, C.H., and Souchelnytskyi, S. (2001). Regulation of Smad signaling by protein kinase C. FASEB J. *15*, 553–555.

Yang, Y., Pan, X., Lei, W., Wang, J., and Song, J. (2006). Transforming growth factor-beta1 induces epithelial-to-mesenchymal transition and apoptosis via a cell cycle-dependent mechanism. Oncogene *25*, 7235–7244.

Zawel, L., Dai, J.L., Buckhaults, P., Zhou, S., Kinzler, K.W., Vogelstein, B., and Kern, S.E. (1998). Human Smad3 and Smad4 are sequence-specific transcrip-tion activators. Mol. Cell *1*, 611–617.

Zhang, J., Yang, P.L., and Gray, N.S. (2009). Targeting cancer with small mole-cule kinase inhibitors. Nat. Rev. Cancer *9*, 28–39.

Zhao, D., and DePinho, R.A. (2017). Synthetic essentiality: targeting tumor suppressor deficiencies in cancer. Bioessays *39*, 1700076.

Zhao, M., Mishra, L., and Deng, C.X. (2018). The role of TGF-beta/SMAD4 signaling in cancer. Int. J. Biol. Sci. *14*, 111–123.

Zhuang, M., Calabrese, M.F., Liu, J., Waddell, M.B., Nourse, A., Hammel, M., Miller, D.J., Walden, H., Duda, D.M., Seyedin, S.N., et al. (2009). Structures of SPOP-substrate complexes: insights into molecular architectures of BTB-Cul3 ubiquitin ligases. Mol. Cell *36*, 39–50.

STAR★METHODS

KEY RESOURCES TABLE

REAGENT or RESOURCE	SOURCE	IDENTIFIER
Antibodies		
Tb cryptate-conjugated mouse monoclonal anti-Flag antibody	Cisbio Bioassays	Cat# 61FG2TLB
D2-conjugated anti-HIS antibody	Cisbio Bioassays	Cat# 61HISDLF
Mouse monoclonal anti-FLAG-HRP antibody	Sigma-Aldrich	Cat# A8592; RRID: AB_439702
Rabbit polyclonal anti-GST-HRP antibody	Sigma-Aldrich	Cat# A7340; RRID: AB_258340
Mouse monoclonal anti-β-Actin antibody	Sigma-Aldrich	Cat# A5441; RRID: AB_476744
Rabbit monoclonal anti-p21 antibody	Cell signaling	Cat# 2947S; RRID: AB_823586
Mouse monoclonal anti-p15 antibody	Santa Cruz	Cat# sc–271791; RRID: AB_10709436
SMAD4 (D3M6U) Rabbit mAb	Cell signaling	Cat# 38454; RRID: AB_2728776
SMAD3 mouse monoclonal Antibody (38-Q)	Santa Cruz	Cat# sc-101154; RRID: AB_1129525
Mouse Anti-Rabbit IgG (Light-Chain Specific) (D4W3E) mAb (HRP Conjugate)	Cell signaling	Cat# 93702; RRID: AB_2800208
Peroxidase AffiniPure Goat Anti-Rabbit IgG(H+L) secondary antibody	Jackson ImmunoResearch	Cat# 111-035-003
Peroxidase AffiniPure Goat Anti-Mouse IgG(H+L) secondary antibody	Jackson ImmunoResearch	Cat# 115-035-003
Chemicals, Peptides, and Recombinant Proteins		
Recombinant Human TGF-beta 1 Protein	R&D Systems	Cat# 240-B
Ro-31-8220	Cayman	Cat# 138489-18-6
Go-6983	Cayman	Cat# 133053-19-7
Ro-31-7549	Cayman	Cat# 138516-31-1
Ro-31-8425	Cayman	Cat# 145317-11-9
Ro-32-0432	Cayman	Cat# 145333-02-4
UCN-1028c	Cayman	Cat# 121263-19-2
PKC-412	Cayman	Cat# 120685-11-2
EEBL	Emory ECBDC (Mo et al., 2019)	N/A
FuGENE	Promega	Cat# E2311
SBE4-Luc	gift from Bert Vogelstein (Zawel et al., 1998)	Addgene plasmid # 16495
Dual-Glo luciferase kit	Promega	Cat# E2920
Oligonucleotides		
p21-F: 5′-ATGTGTCCTGGTTCCCGTTTC-3′;	IDT	N/A
p21-R: 5′-CATTGTGGGAGGAGCTGTGA-3′;	IDT	N/A
p15-F: 5′- GGACTAGTGGAGAAGGTGCG-3′;	IDT	N/A
p15-R: 5′-GGGCGCTGCCCATCATCATG-3′;	IDT	N/A
GAPDH-F: 5′-GAAGGTGAAGGTCGGAGT-3′;	IDT	N/A
GAPDH-R: 5′-GAAGATGGTGATGGGATTTC-3′.	IDT	N/A
Critical Commercial Assays		
CellTiter-Blue® Cell Viability Assay	Promega	Cat# G8081
Experimental Models: Cell Lines		
HCT116	ATCC	Cat# CCL-247; RRID: CVCL_0291
HEK293T	ATCC	Cat# CRL-3216; RRID: CVCL_0063
SW48	ATCC	Cat# CCL-231; RRID: CVCL_1724
DLD-1	ATCC	Cat# CCL-221; RRID: CVCL_0248

Continued

REAGENT or RESOURCE	SOURCE	IDENTIFIER
SW403	ATCC	Cat# CCL-230; RRID: CVCL_0545
SW480	ATCC	Cat# CCL-228; RRID: CVCL_0546
SW620	ATCC	Cat# CCL-227; RRID: CVCL_0547
C2BBe1	ATCC	Cat# CRL-2102; RRID: CVCL_1096
Caco-2	ATCC	Cat# HTB-37; RRID: CVCL_0025
RCM-1	JCRB Cell Bank	Cat# JCRB0256; RRID: CVCL_1648
Software and Algorithms		
Graphpad Prism	Graphpad; v7	https://www.graphpad.com/scientific-software/prism/

RESOURCE AVAILABILITY

Lead contact
Further information and requests for resources and reagents should be directed to and will be fulfilled by the Lead Contact, Haian Fu (hfu@emory.edu).

Materials availability
Plasmids generated in this study are available upon request to the Lead Contact. Other materials are available through commercial sources (see Key Resource Table)

Data and code availability
Analyzed small molecule screening data sets are available through CTD^2 data portal (https://ocg.cancer.gov/programs/ctd2/data-portal).

EXPERIMENTAL MODEL AND SUBJECT DETAILS

All cell lines were incubated at 37°C in humidified conditions with 5% CO_2. Human embryonic kidney 293T cells (HEK293T; ATCC, CRL-3216) and human colorectal carcinoma HCT116 cells (ATCC, CCL-247) were maintained in Dulbecco's Modified Eagle's Medium (DMEM; Corning, #10-013-CV). The isogenic SMAD4 genetic knockout (SMAD4 null (-/-)) HCT116 cells were purchased from Horizon Discovery (#HD 104-005). The isogenic $SMAD4^{R361H}$ cells were generated by lentivirus-transduction of $SMAD4^{R361H}$ plasmid in the SMAD4 null cells. TGFBRII gene was stably expressed in this set of isogenic HCT116 cells. Human colorectal adenocarcinoma cells with various SMAD4 genetic status were purchased and authenticated by sequencing (MacGrogan et al., 1997; Woodford-Richens et al., 2001). SW48 (female; ATCC, CCL-231), DLD-1 (male; ATCC, CCL-221), C2BBe1 (male; ATCC, CRL-2102), Caco-2 (male; ATCC, HTB-37), SW403 (femail; ATCC, CCL-230), SW480 (male; ATCC, CCL-228), SW620 (male; ATCC, CCL-227) and RCM-1 (female; JCRB Cell Bank, JCRB0256) were cultured in Roswell Park Memorial Institute(RPMI) 1640 medium. Cell culture medium was supplemented with 10% fetal bovine serum (ATLANTA biologicals, #S11550) and 100 units/ml of penicillin/streptomycin (Cell Gro, Cat# 30-002-CI).

METHOD DETAILS

Molecular cloning and mutagenesis
The WT SMAD3 (Clone# IOH27044) and SMAD4 (Clone# IOH3638) genes in pDONR221 plasmid were gifted from Drs. Gordon Mill and Yiu Huen Tsang at Oregon Health Science University. The SMAD4 point mutations, including R361H and D351H, were introduced using QuikChange Lightning Site-Directed Mutagenesis Kit (Agilent Technologies) and the SMAD4 pDONR221 plasmid as DNA template and the following primers: R361H forward primer (5'-CTTCTGGAGGAGATCACTTTTGTTTGGGTCAAC-3'), D351H forward primer (5'CCCTATTGTTACTGTTCATGGATACGTGGACCC-3'), and corresponding reverse complementary primers. Gateway cloning (Invitrogen) was used to generate GST-tagged, Venus-flag-tagged, Flag-tagged and 6XHis-tagged plasmids. The vector backbones are pDEST27 vector (Invitrogen) for GST-tag, pDEST26 (Invitrogen) for 6XHis tag, pSCM167 for Venus-flag-tag, pcDNA3.2-V5-dest for Flag-tag constructs, and pHAGE lentiviral vector for virus packaging. All plasmids generated were confirmed by sequencing.

Time-resolved fluorescence resonance energy transfer (TR-FRET) assay
TR-FRET assays were performed using cell lysate from HEK293T cells expressing Flag-tagged SMAD3 and His-tagged SMAD4 WT or MUT proteins. The FRET buffer used throughout the assay contains 20 mM Tris-HCl, pH 7.0, 50 mM NaCl, and 0.01% nonidet

P-40 (NP-40). Briefly, the HEK293T cells were transiently co-transfected with Flag-tagged SMAD3 (1 μg/well) and His-tagged SMAD4 WT (1 μg/well) or MUT (1 μg/well) plasmids in the 6-well plate. Linear polyethylenimines (PEIs, Polysciences, PA Cat # 23966) were used as transfection reagent at 3:1 (PEI/plasmid mass) ratio. Forty-eight hours after transfection, cell lysates were prepared in 200 μl lysis buffer containing 150 mM NaCl, 10 mM HEPES pH 7.5, 1% nonident P-40 (IGEPAL CA-630, Sigma-Aldrich), 5 mM sodium pyrophosphate, 5 mM NaF, 2 mM sodium orthovanadate, 10 mg/L aprotinin, 10 mg/L leupeptin and 1mM PMSF. To determine the optimal assay window for HTS, the cell lysates concentration dependent TR-FRET assays were performed in black 384-well plates (Corning Costar, #3573). A 15 μl of stock cell lysate was 2-fold serially diluted in FRET buffer and mixed with 15 μl mixture of fluorophore-conjugated antibodies. The total volume for each well was 30 μl containing the cell lysate, anti-FLAG M2-Tb cryptate antibody (Cisbio 61FG2TLF, 1:1000 dilution) and anti-6XHIS-D2 antibody (Cisbio 61HISDLF, 1:500 dilution). The plate was centrifuged at 1,000 rpm for 5 min and incubated at 25 °C for 30 min. TR-FRET signals were measured using the BMG Labtech PHERAstar *FSX* reader with the HTRF optic module (excitation at 337 nm, emission A at 665 nm, emission B at 620 nm, integration start at 50 μs, integration time for 150 μs and 8 flashes per well). All FRET signals were expressed as a TR-FRET ratio: $F_{665nm}/F_{620nm} \times 10^4$.

uHTS TR-FRET screening for small molecule PPI inducer discovery
Ultra-high-throughput screening (uHTS) for small molecule PPI inducer discovery was performed using the TR-FRET assay in the black 1536-well plate (Corning Costar, #3724) with a total volume of 5 μL in each well. The amount of cell lysate and antibodies were scaled down proportionally from the conditions with the optimal assay window identified from 384-well plate. Briefly, 5 μL solutions containing cell lysate (23 μg/ml) and antibodies at desired concentrations were dispensed in the 1536-well plate using a Multidrop Combi Reagent Dispenser (ThermoScientific). The last column was used as the empty vector background control. Subsequently, the 2036 Emory Enriched Bioactive Library (EEBL) compounds (100 nl) were added into wells in each plate using Biomek NXP Automated Workstation (Beckman) from a compound stock plate to give the final concentration of 20 μM. The final DMSO concentration was 2% (v/v) in samples with compound treatment. Each sample was tested with single point. After overnight incubation at 4 °C, FRET signal was measured using the BMG Labtech PHERAstar *FSX* reader with the HTRF optic module. To evaluate the performance of the assay for HTS, Z' factor and signal-to-background(S/B) ratio was calculated for the TR-FRET titration experiment according to the following equations:

$$Z' = 1 - \frac{3 \times SD_{PPI} + 3 \times SD_{vector}}{FRET_{PPI} - FRET_{vector}}$$

$$S/B = FRET_{PPI}/FRET_{vector}$$

where SD_{PPI} and SD_{vector} are standard deviations, and $FRET_{PPI}$ and $FRET_{vector}$ represent the TR-FRET signal from lysate containing His-SMAD4^{R361H} and Flag-SMAD3 or empty Flag-vector controls, respectively. S/B suggests the signal window of the assay and Z' factor reflects the robustness of the assay for HTS. A Z' factor between 0.5 and 1 indicates a robust assay and suit for HTS. Screening data were analyzed using Bioassay software from CambridgeSoft (Cambridge, MA). The effect of compound on PPI modulation was quantified as the change of TR-FRET signal (ΔTR-FRET) upon compound treatment using the equation 100x(FRET$_{compound}$-FRET$_{DMSO}$)/FRET$_{DMSO}$, where FRET$_{compound}$ and FRET$_{DMSO}$ are the TR-FRET signals from PPI in the presence of library compound or DMSO with background FRET$_{vector}$ subtracted. Cutoff of ΔTR-FRET ≥ 2SD$_{PPI}$ was used to prioritize the positive hits.

GST pull-down assay
To validate the hits from the pilot screening, we performed orthogonal GST pull-down assay using cell lysate from the HEK293T cells transfected with Venus-flag-SMAD3 and GST-SMAD4-WT or MUT. After 48hrs of transfection, the cells were lysed by the 0.5% Triton X-100 Lysis buffer (20 mM Tris-HCl, 150 mM NaCl, 5% glycerol, 0.5% Triton X-100, 2 mM EDTA) and incubated with compounds for 3h rotating at 4°C, and then incubated with glutathione-conjugated beads (GE 17527901) for 2h at 4°C. Beads were washed three times with the 0.5% Triton Lysis buffer and eluted by boiling in sodium dodecyl sulfate (SDS) sample buffer (ThermoFisher) and subjected to western blot analysis.

Co-immunoprecipitation (co-IP) with endogenous proteins
The immunoprecipitation was performed using cell lysate from colon cancer cell line HCT116 and RCM-1 harboring SMAD4 WT and R361H respectively. Briefly, cells were seeded in 100 mm cell culture dish and treated with 10 μM Ro31-8220 or DMSO control for 8h. The cell lysate was obtained in PBS with sonication. For each co-immunoprecipitation, lysates containing ~1.5 mg of total proteins were used and the antibody/lysate mixtures were incubated overnight at 4 °C. Then protein A/D agarose beads were added to the mixture followed by incubation at 4 °C for another 4 h. Beads were washed four times with PBS, and proteins were eluted with SDS-PAGE sample buffer and analysed with indicated antibodies using western blot.

Cellular thermal shift assay (CETSA)
The SMAD3 and SMAD4 protein stability were measured using the CETSA assay by treating human colon cancer cells with compound at desired concentrations. Briefly, HCT116 (SMAD4^{WT}) and RCM1 (SMAD4^{R361H}) were plated into 100 mm dishes at 60%

confluency and treated with 10 μM Ro31-8220 for 8h. The cell pellet was collected in 1mL PBS and aliquoted into PCR tubes (95 μl/tube) for thermal denaturation at 45∼65 °C) on the thermal cycler for 3 min. After thermal denaturation, cell lysate was obtained by three freeze-thaw cycles between liquid nitrogen and 25 °C, followed by centrifugation at 20,000g for 20 min at 4 °C to pellet cell debris together with precipitated and aggregated proteins. The soluble proteins were then detected by SDS-PAGE and western blot.

Protein stability assay
RCM-1 cells were grown in 24-well plates for 24 hrs and then were treated with 100 μg/mL cycloheximide (2112, Cell Signaling). At the indicated times. 100 μl of 2X SDS-PAGE sample buffer was added and the cells were scraped from the wells, boiled for 5 minutes, then cell lysates were stored at -80°C. After all lysates were collected, each sample was loaded onto a 10% SDS-PAGE gel and then analyzed by Western blotting with anti-SMAD4 antibody to monitor SMAD4 protein level. Protein expression was quantified from the Western blot using ImageJ software for analysis, SMAD4 levels were normalized to β-Actin protein levels. Assays were performed three times.

Western blot
Proteins in the SDS sample buffer were resolved by 10% SDS polyacrylamide gel electrophoresis (SDS-PAGE) and were transferred to nitrocellulose filter membranes at 100 V for 2h at 4°C. After blocking the membranes in 5% nonfat dry milk in 1×TBST (20mM Tris-base, 150mM NaCl, and 0.05% Tween 20) for 1 hour at room temperature, membranes were blotted with the indicated antibodies at 4°C overnight. Membranes were washed by 1×TBST for three times, 15 minutes each time. SuperSignal West Pico PLUS Chemi-luminescent Substrate (Thermo, #34580) and Dura Extended Duration Substrate (Thermo, #34076) were used for developing membranes. The luminescence images were captured using ChemiDoc™ Touch Imaging System (Bio-Rad).

SMAD binding element (SBE) luciferase reporter assay
The SMAD3/SMAD4 complex transcriptional activity was measured using the SBE-luciferase reporter system. Colon cancer cell HCT116 and RCM-1 were used to measure the luciferase activity in SMAD4 WT and R361H mutated conditions, respectively. Cells were plated in 6-well plate and co-transfected with SBE4-Luc plasmid (1 μg, Addgene,16495) and pDEST26-Renilla plasmid (0.1 μg) using FuGENE® HD (Promega, Cat# E2312). Twenty-four hours after transfection, the cells were pre-treated with the selected compound was 6h followed by TGF-β stimulation for additional 18h. Renilla and Firefly luciferase activities were measured by Envision Multilabel plate reader (PerkinElmer) using and Dual-Glo luciferase kit (Promega, Cat# E2920) according to the manufacturer's instructions. The normalized luminescence was calculated as the ratio of luminescence of Firefly luciferase over the luminescence of Renilla luciferase.

Transcriptome analysis and quantitative polymerase chain reaction (qPCR)
TGFβ and compound-induced transcriptome change were measured and analyzed using mRNA sequencing service from Novogene Co., Ltd.. Briefly, the isogenic HCT116 colon cancer cells harboring differential SMAD4 genetic mutations were pretreated with the compound for 6h followed by TGFβ stimulation for 18 h. The total mRNA was purified using the E.Z.N.A total RNA kit (Omega Bio-tek Cat# R6834-01) followed by DNase I (Invitrogen, Cat# 18068-015) treatment and then heat inactivation at 65°C for 10 minutes in the presence of 2 mM EDTA. cDNA was synthesized using 250 ng of total RNA and the SuperScript III first-strand cDNA synthesis kit (Invitrogen, Cat# 18080-051) and sequenced using Illumina next-generation sequencing platform. The cDNA were prepared similarly for other colon cancer cells and used for qPCR analysis of the selected differential expression genes, such as p15 and p21. The following primers were ordered from IDT (Coralville, IA, USA):

p21-F: 5′-ATGTGTCCTGGTTCCCGTTTC-3′;
p21-R: 5′-CATTGTGGGAGGAGCTGTGA-3′;
p15-F: 5′- GGACTAGTGGAGAAGGTGCG-3′;
p15-R: 5′-GGGCGCTGCCCATCATCATG-3′;
GAPDH-F: 5′-GAAGGTGAAGGTCGGAGT-3′;
GAPDH-R: 5′-GAAGATGGTGATGGGATTTC-3′.

The qPCR was performed and analyzed using the Eppendorf Mastercycler® Realplex system (Eppendorf) through 45 cycles of 95°C for 15 s, 55°C for 15 s, and 72°C for 20 s, and detected using SsoAdvanced Universal SYBR Green Supermix reagent (Bio-Rad, Cat#, 172-5271). The normalized target gene expression (ΔCt, delta cycle threshold) was calculated as ΔCt = Ct(GAPDH) - Ct(gene), where Ct(GAPDH) and Ct(gene) are the Ct value for GAPDH and target genes, respectively. The TGFβ induced change of target gene expression (ΔΔCt) was calculated as ΔΔCt = ΔCt(+TGF-β)-ΔCt (-TGF-β), where ΔCt(+TGF-β) and ΔCt(-TGF-β) are the ΔCt of target gene with and without TGF-β stimulation, respectively. The fold of change (FOC) of the mRNA expression was determined as $2^{-\Delta\Delta Ct}$.

Gene set enrichment analyses (GSEA)
Gene Set Enrichment Analysis (GSEA) was performed by the GSEA() function of the GSEABase package (https://www.bioconductor.org/packages/release/bioc/html/GSEABase.html) in R Studio. The indicating gene sets from either KEGG or Hallmark molecular signatures database were selected as the reference gene sets. We ranked the genes of indicating pathways in accordance with the differential expression within treatment and control groups. We calculated the normalized enrichment score (NES) to reflect the degree

in which a set of genes is overrepresented at the extremes (top or bottom) among the entire ranked list. All GSEA analyses were performed strictly according to the instruction (https://www.bioconductor.org/packages/release/bioc/vignettes/GSEABase/inst/doc/GSEABase.pdf). As for statistical significance, |NES|>1 with a P value and False discovery rate (FDR) <0.05 was considered as an enriched gene set.

Cell cycle analysis

Colon cancer cells were pre-synchronized in serum-free medium for 24 hours. After 24-h serum starvation, full culture media with 10% FBS were replaced for the following TGFβ and/or compound treatment. After 24-treatment, cells were trypsinized, harvested, washed, and then fixed in 70% ethanol overnight at 4°C. Before flow cytometry analysis, the cells were then treated with 1 mg/ml of RNase for 30 min at 37°C, and then stained with 40 μg/ml of PI for 30 min. A total of 5,000 cells/sample were analyzed using a Guava flow cytometer (Millipore). Data were evaluated using Guava Cell Cycle software.

Colony formation assay

Colony formation assay was performed as we described previously(Sun et al., 2005). Briefly, cells (single-cell suspension) were plated in 6-well plates at a density of 1,000 to 2,000 cells per well. On the second day, cells were treated with TGF-β, Ro-31-8220 or Go-6983 or in combination. Every 3 days, the medium was replaced with fresh medium containing the corresponding agents. After a 15-day treatment, the medium was removed, and cell colonies were stained with crystal violet dye as described. Images were acquired using ChemiDoc Touch Imaging system (Biorad) and colony area were quantified using ImageJ Colony Area plugin(Guzman et al., 2014).

Cell viability assay

Cell Titer Blue (Promega, G8081) was added to each well. The plates were incubated for desired time at 37°C to allow the generation of sufficient signal within the linear range. The fluorescence intensity of each well was read using an PHERAstar FSX multi-mode plate reader (Ex 545 nm, Em 615 nm; BMG LABTECH). Cells containing medium alone were used as blank control for background correction.

QUANTIFICATION AND STATISTICAL ANALYSIS

All the assays were performed and repeated three times. The data quantification and statistic of Student's t-test was performed using the GraphPad Prism software. See the Quantification and Statistical Details in the corresponding methods, figure legends and results.